Supplementary Material for

Synergistic use of SMAP and OCO-2 data in assessing the responses of ecosystem productivity to the 2018 U.S. drought

Xing Li[a], Jingfeng Xiao[a*], John S. Kimball[b], Rolf H. Reichle[c], Russell L. Scott[d], Marcy E. Litvak[e], Gil Bohrer[f], Christian Frankenberg[g,h]

[a] Earth Systems Research Center, Institute for the Study of Earth, Oceans, and Space, University of New Hampshire, Durham, NH 03824, USA

[b] Numerical Terradynamic Simulation Group, College of Forestry & Conservation, University of Montana, Missoula, MT, USA

[c] Global Modeling and Assimilation Office, NASA Goddard Space Flight Center, Greenbelt, MD, 20771 USA

[d] Southwest Watershed Research Center, USDA-ARS, Tucson, AZ 85719, USA

[e] Department of Biology, University of New Mexico, Albuquerque, NM 87131, USA

[f] Department of Civil, Environmental and Geodetic Engineering, Ohio State University, Columbus, OH 43210, USA

[g] Division of Geological and Planetary Sciences, California Institute of Technology, Pasadena, CA 91125, USA

[h] Jet Propulsion Laboratory, California Institute of Technology, Pasadena, CA 91109, USA

*Email: j.xiao@unh.edu

This supplementary material contains ten figures (Fig. S1-S10) and two tables (Table S1 and S2).

Supplementary Methods

Characterizing the 2018 drought based on a longer time period

The short time period (2015–2018) used for anomaly calculation may impact the results, especially for contextualizing the "normal" years. Therefore, we also used a longer time period (2000–2018) to calculate the anomalies of GOSIF and VPD due to their longer data record. The results based on the longer time period showed that among the four years (2015-2018), only 2018 showed widespread positive anomalies in VPD for the southwestern US (Fig. S1), while other years were nearly drought-free, suggesting that 2018 was indeed a severe drought year regardless of the reference period used (2015-2018 or 2000-2018). The maps of VPD and GOSIF anomalies based on either short or longer time period detected the severe drought in 2018 over the southwestern US, although the anomalies were enhanced over the shorter reference period (Fig. S2). Although different time periods were used to calculate the anomalies, the SIF had similar responses to VPD anomalies especially for the dryland-dominated U.S. Southwest (Fig. S2).

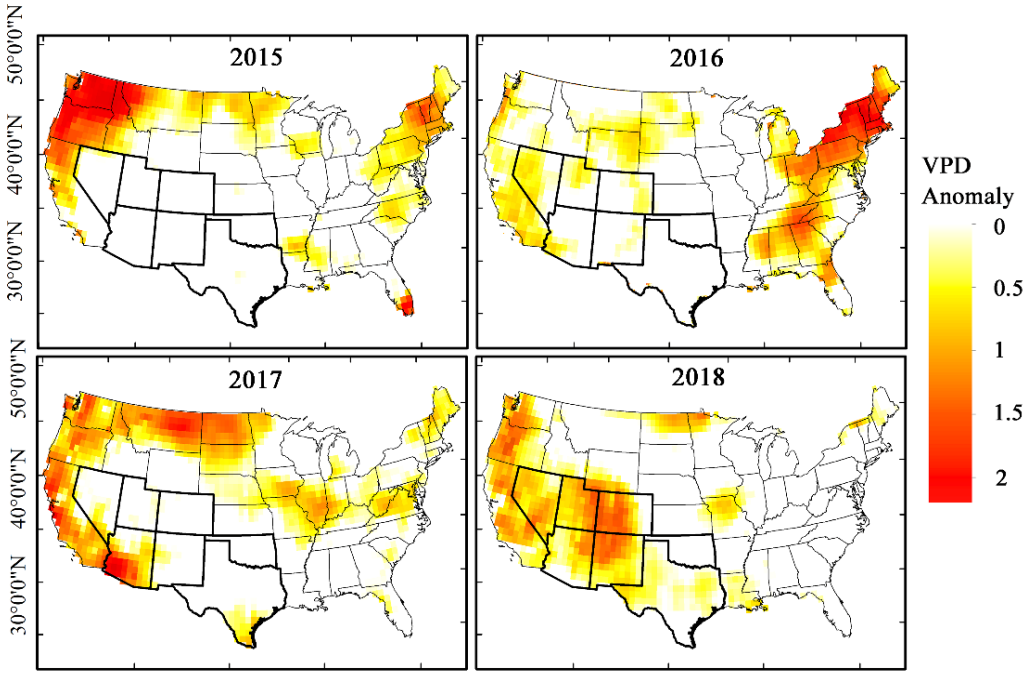

Fig. S1. The spatial patterns of growing-season averaged standardized anomalies of VPD in 2015, 2016, 2017, and 2018 over the CONUS. The anomalies were calculated based on longer time period from 2000 to 2018. The boundary of the seven states in the southwestern US is highlighted.

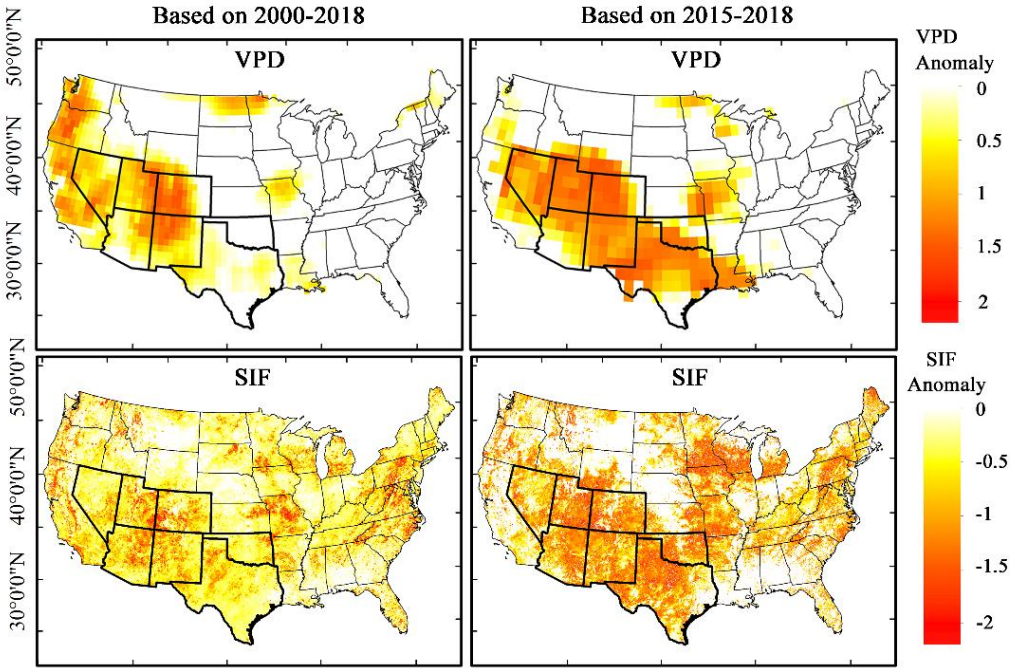

Fig. S2. The spatial patterns of growing-season averaged standardized anomalies of GOSIF and VPD in 2018 over the CONUS. The left column was calculated based on longer time period from 2000 to 2018; while the right column was based on short time period from 2015 to 2018.

SMAP pixel-mean GPP versus PFT-specific GPP

We compared the pixel-mean SMAP GPP and PFT-specific SMAP GPP for the four selected sites, and found that the difference between the two types of GPP was negligible for three out of four sites (except for US-Vcm; Fig. S3), suggesting that three sites are generally consistent with the overlying 9-km grid cell. The US-Vcm site is recovering from recent fire disturbance and is dominated by elderberry and aspen seedlings, while the GPP of the overlying SMAP 9km grid cell is dominated by surrounding evergreen needleleaf forests. The L4C sub-grid PFT-specific GPP for shrubland was therefore selected for the tower comparison at this site rather than the GPP for evergreen needleleaf forests.

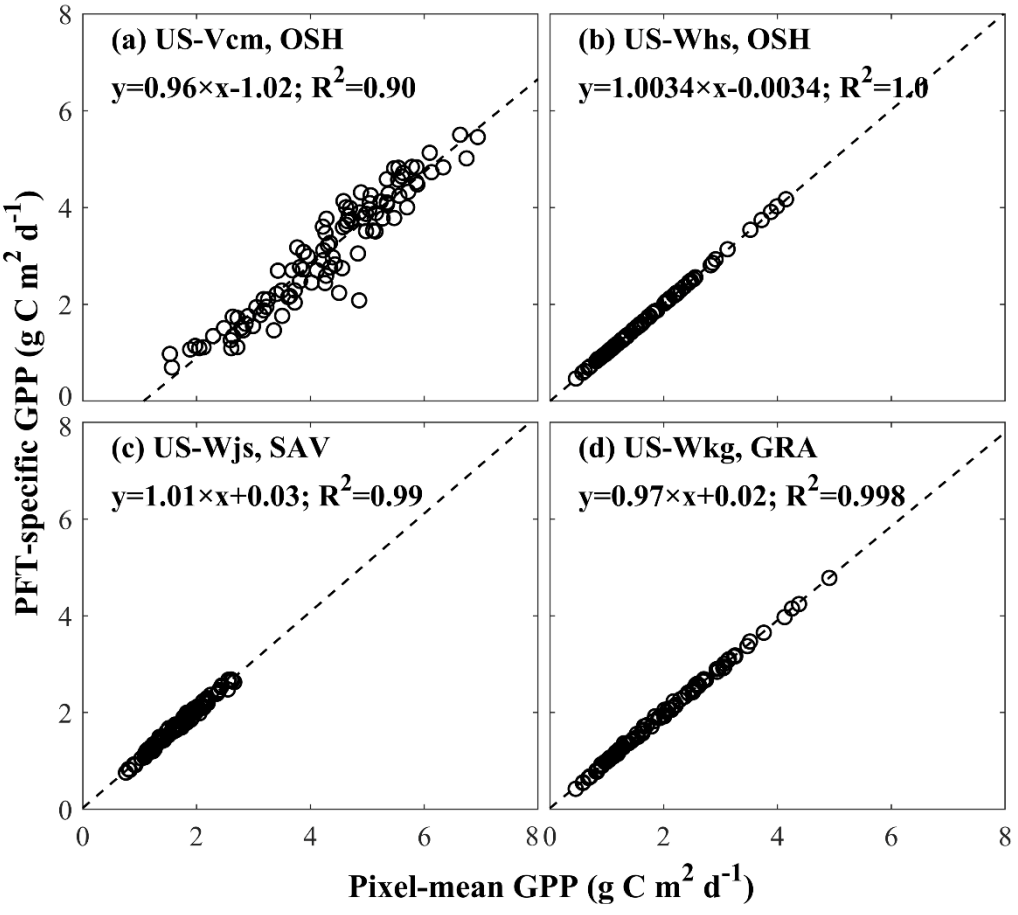

Fig. S3. The comparison between SMAP pixel-mean GPP and PFT-specific GPP for four EC

flux sites. The pixel-mean GPP integrated information from the 9km pixel regardless of the land cover type, while the PFT-specific GPP indicated that the extracted GPP was only aggregated by sub-pixels having same land cover type with target flux tower.

To complement SMAP GPP and GOSIF, the coarse-resolution SIF that were directly aggregated from discrete OCO-2 SIF soundings, MODIS EVI, and MODIS GPP were also used as proxies of ecosystem productivity to understand the impact of drought.

OCO-2 SIF

The OCO-2 SIF was extracted from the OCO-2 Level 2 bias-corrected SIF files (OCO2_L2_Lite_SIF, V8r) (OCO-2 Science Team/Michael Gunson, 2017). The OCO-2 instrument provides SIF estimates with higher spatial resolution along orbits (i.e., 1.3 × 2.25 km^2) (Frankenberg et al. 2014) than previous GOSAT and GOME-2 SIF. However, due to the sparse sampling strategy of OCO-2 (Li and Xiao 2019a; Sun et al. 2018), we generated a coarse-resolution SIF (1.5°, monthly) from 2015 to 2018 to guarantee global coverage using the discrete and non-gridded SIF retrievals. Since varying viewing zenith angle (VZA) may affect the magnitude of SIF (Li et al. 2018a), we only used SIF retrievals with VZA lower than 45°. The instantaneous SIF at 757 nm was converted to a daily scale using the daily correction factor included in the Lite SIF files. For examining the consistency among productivity proxies, we calculated the correlation between GOSIF and SMAP GPP (or OCO-2 SIF). The comparison between GOSIF and the coarse-resolution OCO-2 SIF was only conducted at monthly time scale owing to the comparatively sparse OCO-2 sampling. The growing-season averaged anomaly of OCO-2 SIF was not calculated because of large

spatial gaps existing in the monthly data and data missing in August 2017.

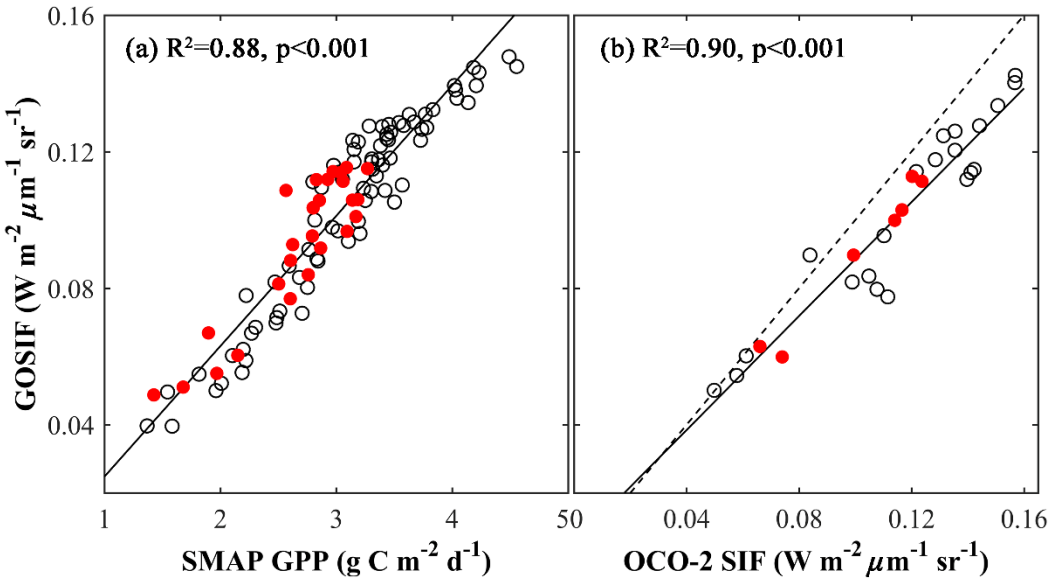

Fig. S4. The consistency between three productivity measures in growing seasons from 2015 to 2018. (a) shows the 8-day GOSIF versus SMAP GPP; (b) shows the monthly GOSIF versus coarse-resolution OCO-2 SIF. The data in the 2018 drought year are shown with filled red circles.

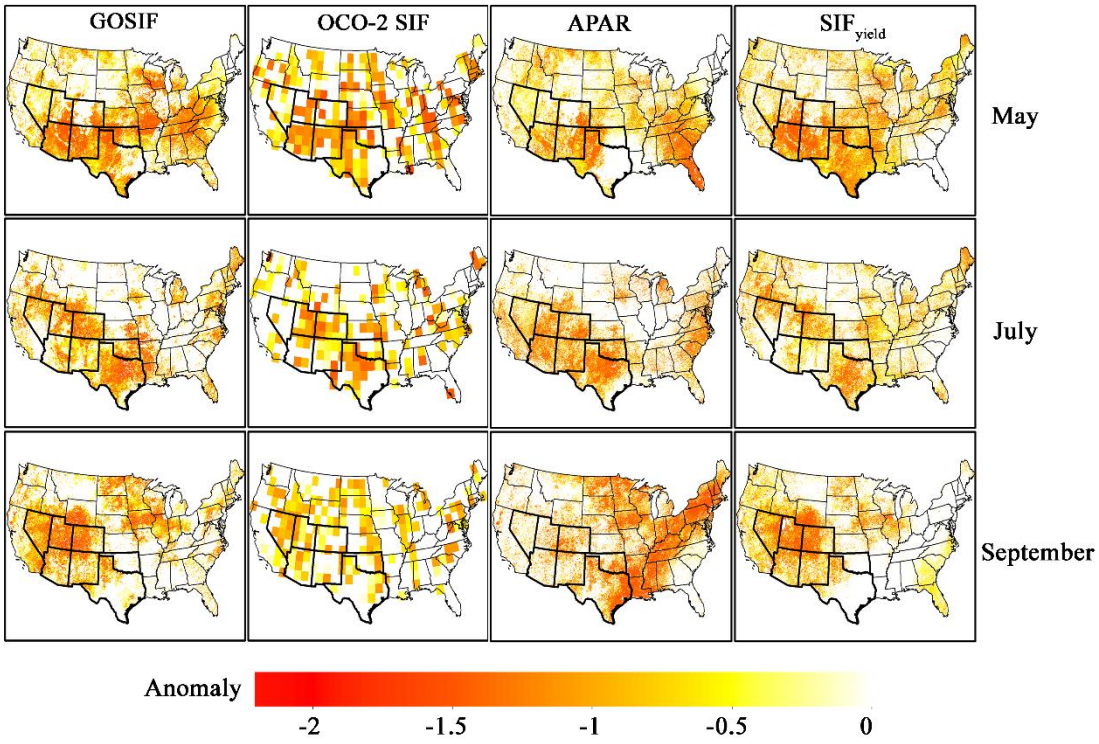

Fig. S5. The spatial pattern of monthly anomalies of GOSIF, OCO-2 SIF, APAR, and SIF_{yield} in May, July, and September 2018 over the CONUS. The boundary of the seven states in the southwestern U.S. is highlighted.

MODIS GPP and EVI

MOD17 GPP model (Zhao et al. 2005) uses a similar LUE model and inputs as the SMAP L4C product, except that VPD provides the sole moisture control on productivity. Here, we obtained the gap-filled 8-day, 500 m MODIS GPP (MOD17A2HGF Version 6) from https://lpdaac.usgs.gov/products/mod17a2hgfv006/.

At the ecosystem scale, we examined the 8-day variations of MODIS GPP and EVI in the 2018 drought year relative to their multi-year average, and assessed whether they could also characterize the drought-induced reduction of tower GPP. The EVI used in this study was derived and calculated from the daily MODIS nadir surface reflectance product (MCD43C4, Collection 6, 0.05°) over the period 2015–2018.

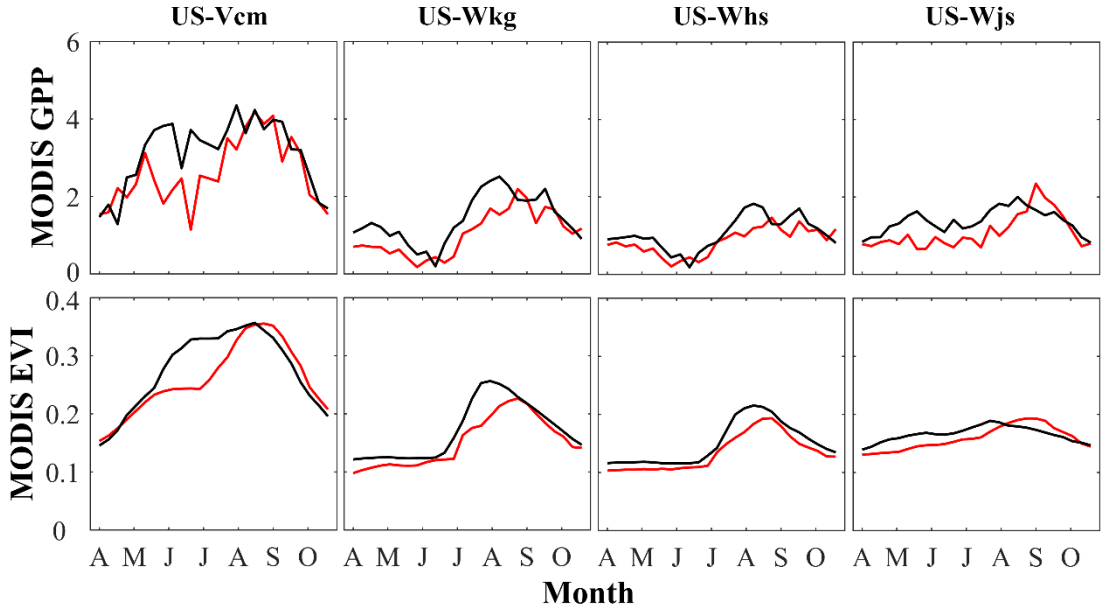

Fig. S6. The seasonal cycles of MODIS GPP (g C m^{-2} d^{-1}) and EVI at four EC flux sites. The red lines stand for the 8-day variations in the growing season during the 2018 drought year, while the black lines denote the averages of normal years.

Validating the relationships between flux tower GPP and different variables

For the four selected EC flux sites, we first examined the relationships between 8-day tower GPP and different productivity proxies and environmental indicators during the growing season from 2015 to 2018. High correlations between tower GPP and these variables were prerequisite for effectively monitoring the drought-induced variations of GPP based on these variables. The included productivity proxies were GOSIF, SMAP GPP, MODIS GPP, EVI, and APAR; while environmental indicators were SIF_{yield} (SIF/APAR), MODIS LUE term (minimum air temperature scalar × VPD scalar), and SMAP LUE term (minimum air temperature scalar × VPD scalar × landscape freeze/thaw scalar × root zone soil moisture scalar) (Jones et al. 2017). The SMAP LUE term was constructed by specifying additional environmental constraints for frozen landscape conditions and low root zone soil moisture upon the original MODIS LUE term (Jones et al. 2017), which was directly provided by the L4C product, while the MODIS LUE was derived as MODIS GPP divided by APAR. We also compared the tower-based LUE (tower GPP/APAR) with SIF_{yield}, SMAP LUE, and MOSID LUE. These comparisons provided insight into the underlying reasons for the relationship between the tower GPP and satellite productivity metrics. We used the average of a total of nine 500-m GPP pixels in a 3*3 pixel window surrounding each tower site.

Overall, among five productivity proxies (Table S1), GOSIF showed the highest correlations with tower GPP (R^2=0.46-0.80); EVI was also highly correlated with tower GPP (R^2=0.52-0.78); SMAP GPP and MODIS GPP had comparable but lower

correlations. The higher sensitivity of GOSIF to tower GPP compared to two GPP products was contributed by the SIF_{yield}, which better accounted for the variance in tower GPP than the LUE terms from SMAP and MODIS. The stronger GPP-SIF_{yield} relationships resulted from the stronger tower LUE-SIF_{yield} relationships compared with SMAP or MODIS LUE (Table S2). Due to inclusion of soil moisture information, the SMAP LUE had slightly higher sensitivity to tower GPP than MODIS LUE.

Table S1. The correlations between 8-day tower GPP and five productivity proxies and three environmental indicators at four sites. The numbers show the R^2 between tower GPP and each variable. All relationships are statistically significant ($p<0.01$) except for APAR at the US-Wjs site.

Site	**GOSIF**	**SMAP GPP**	**MODIS GPP**	**APAR**	**EVI**	**SIF_{yield}**	**SMAP LUE**	**MODIS LUE**
US-Vcm	0.69	0.53	0.52	0.60	0.57	0.44	0.1	0
US-Whs	0.71	0.70	0.54	0.49	0.67	0.42	0.35	0.13
US-Wjs	0.46	0.29	0.51	0.30	0.52	0.18	0.32	0.23
US-Wkg	0.80	0.74	0.68	0.69	0.78	0.57	0.46	0.19

Table S2. The R^2 values for the linear relationships of tower LUE with SIF_{yield}, SMAP GPP LUE, and MODIS LUE at four sites.

Site	**SIF_{yield}**	**SMAP LUE**	**MODIS LUE**
US-Vcm	0.20	0.11	0.08
US-Whs	0.74	0.47	0.65
US-Wjs	0.05	0	0.01
US-Wkg	0.64	0.52	0.26

Fig. S7 showed the relationships between tower GPP and SMAP GPP (and GOSIF) at four selected EC flux tower sites. The slopes between SMAP GPP and tower GPP were close to 1 for three out of the four sites (US-Vcm, US-Wkg, and US-Whs). The relationship was only weaker for US-Wjs, leading to different slope. We further examined site homogeneity of US-Wjs by using 250m EVI, land cover map from 30m National Land Cover Database (NLCD), and 500m MODIS land cover map (Fig. S8). The 9km SMAP pixel where US-Wjs was located was mainly dominated by grassland and shrubland (Fig. S8a). MODIS land cover map did not well identify the shrubland pixels (Fig. S8b), and classified a significant fraction of grassland pixels which had lower EVI and consequently lower productivity (Fig. S8c) as shrublands. We found that the 9km pixel-mean EVI, grassland EVI, shrubland EVI based on MODIS land cover map (actually largely composed by grassland pixels) were all lower than the EVI at the US-Wjs site (Fig. S8d). The SMAP PFT-specific GPP was calculated based on the MODIS land cover map, and therefore, 9km pixel-mean GPP, grassland GPP and shrubland GPP (largely composed by grassland pixels) all underestimated the GPP of US-Wjs. Although SMAP partly solves the heterogeneity problem for matching the tower site by providing PFT-specific GPP, the GPP may also be affected by the classification accuracy of MODIS land cover map. If NLCD were used to identify shrubland pixels (Fig. S8a), the tower GPP for US-Wjs would not be underestimated since the identified shrubland pixels by NLCD had consistently higher EVI (Fig. S8c). When linking 9km SMAP GPP or 0.05° GOSIF to the flux tower sites, the heterogeneity problem may be inevitable since the

footprints of traditional towers range from several hundred meters to 1 or 2 kilometers. The landscape around US-Wjs is not highly heterogeneous, but the difference between tower GPP of US-Wjs and the GPP from surrounding pixels was still observed. Nevertheless, SMAP GPP and GOSIF could still capture the drought impact on tower GPP (Fig. 8 in the main text). Further enhanced spatial resolution for both SMAP GPP and GOSIF will be more helpful. More sites encompassing a variety of biomes are needed to validate the relationships between SMAP GPP/GOSIF and tower GPP. This can help to understand whether both products systematically under- or over-estimate GPP for certain biomes and promote model improvement in the future.

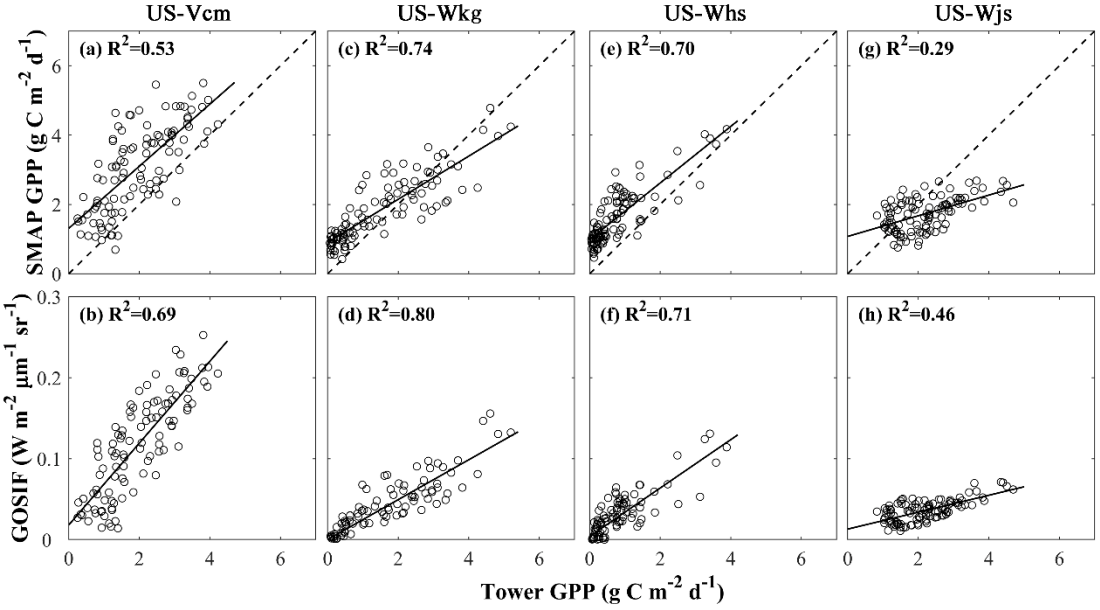

Fig. S7. Relationships of tower GPP with SMAP GPP (*upper panels*) and GOSIF (*lower panels*) at four selected EC flux tower sites. Each circle represents variables at 8-day time scale from April to October over 2015–2018.

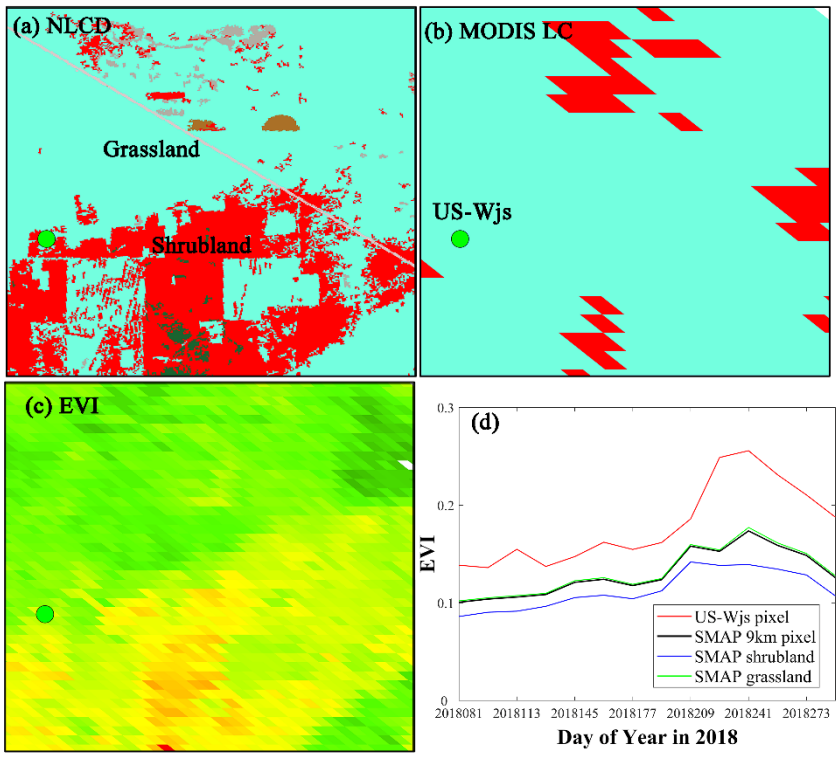

Fig. S8. Land cover and EVI within the 9km SMAP pixel where US-Wjs is located. (a) Land cover from 30m NLCD map; (b) Land cover from 500m MODIS map; (c) 250 m MODIS EVI. The 9km pixel is mainly covered by grassland (cyan) and shrubland (red). (c) Shrubland has higher EVI than grassland (green: low EVI; red: high EVI). (d) shows the EVI for US-Wjs pixel and SMAP 9km averaged and PFT-specific EVI. SMAP calculated PFT-specific GPP based on MODIS land cover map (b), therefore, the real shrubland pixels which had higher EVI were not used, leading to slight underestimation of GPP for US-Wjs.

Soil moisture validation

We obtained surface soil moisture for US-Whs and US-Wkg sites, and found that the SMAP root-zone soil moisture had lower correlations with surface soil moisture possibly due to different depths of soil, but it still captured the negative anomaly of measured soil moisture to a certain degree (Fig. S9). This may account for the stronger relationships between the SMAP LUE and tower GPP relative to the

MODIS LUE, and consequently stronger relationships between SMAP GPP and tower GPP than MODIS GPP (Table S1).

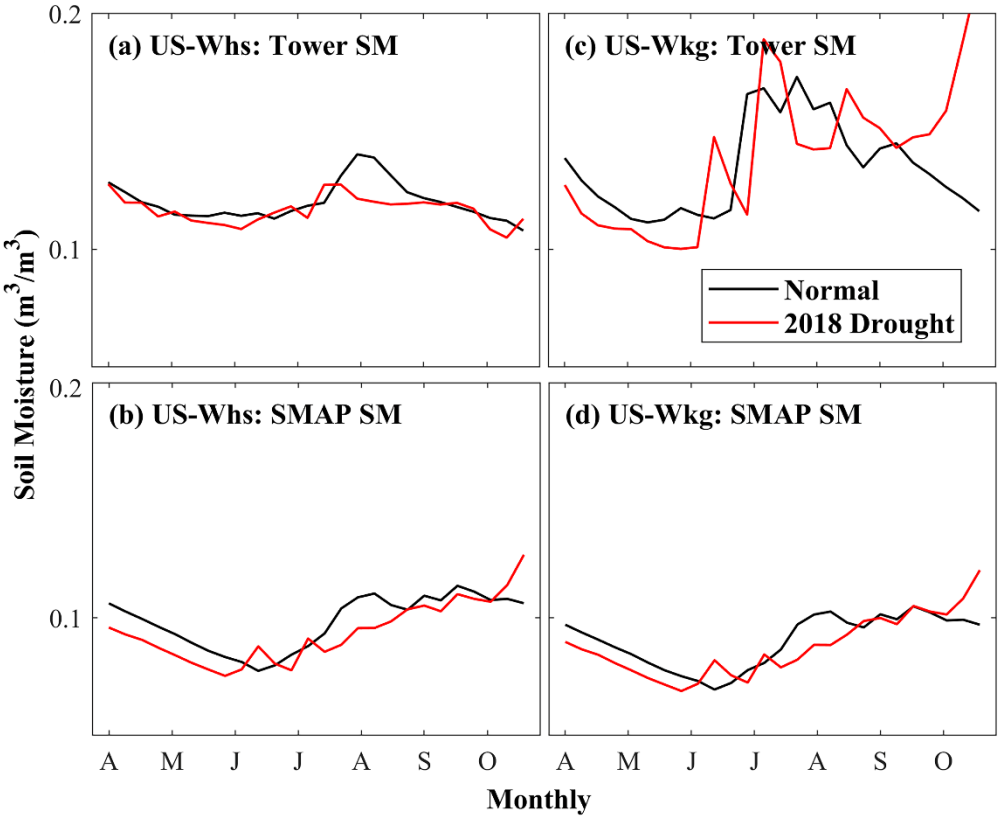

Fig. S9. The seasonal cycles of flux and SMAP soil moisture and (m^3/m^3) for the US-Whs and US-Wkg sites. The red lines stand for the 8-day variations in the growing season during the 2018 drought year, while the black lines denote the averages of normal years.

The impact of drought on irrigated and rainfed crops

For counties that provided data for both rainfed and irrigated crops, we correlated the county-level anomalies of SMAP GPP and GOSIF to those of rain-fed crop yield or irrigated crop yield separately (Fig. S10). We found that the yield of irrigated crops was weakly related to SMAP GPP and GOSIF, while the yield of rainfed crops had much higher sensitivity to the variations of SMAP soil moisture and were thus strongly correlated with SMAP GPP and GOSIF. This confirmed the

findings of previous studies that the rainfed crops were more vulnerable to the climate change or drought than the irrigated crops (Li et al. 2015; Ozelkan et al. 2016).

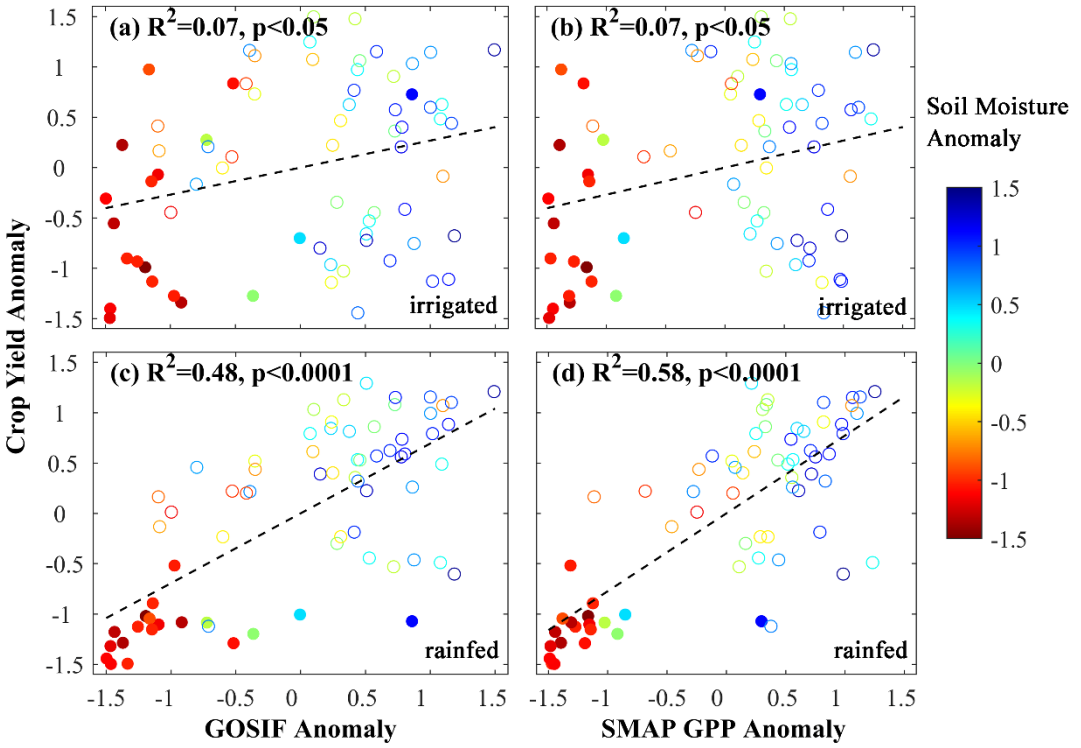

Fig. S10. Relationships of anomalies in crop yield with anomalies in SMAP GPP and GOSIF for irrigated and rainfed crops. Hollow circles represent the anomalies in county-level end of season crop yield against anomalies in county-averaged GPP and GOSIF in normal year (2015-2017), while solid circles denote the 2018 drought year.

References:

Frankenberg, C., O'Dell, C., Berry, J., Guanter, L., Joiner, J., Köhler, P., Pollock, R., & Taylor, T.E. (2014). Prospects for chlorophyll fluorescence remote sensing from the Orbiting Carbon Observatory-2. *Remote Sensing of Environment, 147*, 1-12

Jones, L.A., Kimball, J.S., Reichle, R.H., Madani, N., Glassy, J., Ardizzone, J.V., Colliander, A., Cleverly, J., Desai, A.R., & Eamus, D. (2017). The SMAP Level 4 Carbon Product for Monitoring Ecosystem Land–Atmosphere CO 2 Exchange. *IEEE Transactions on Geoscience and Remote Sensing, 55*, 6517-6532

Li, X., & Xiao, J. (2019a). A Global, 0.05-Degree Product of Solar-Induced Chlorophyll Fluorescence Derived from OCO-2, MODIS, and Reanalysis Data. *Remote Sensing, 11*, 517

Li, X., Xiao, J., & He, B. (2018a). Chlorophyll fluorescence observed by OCO-2 is strongly related to gross primary productivity estimated from flux towers in temperate forests. *Remote Sensing of Environment, 204*, 659-671

OCO-2 Science Team/Michael Gunson, A. E. (2017). OCO-2 Level 2 bias-corrected solar-induced fluorescence and other select fields from the IMAP-DOAS algorithm aggregated as daily files, Retrospective processing V8r. Greenbelt, MD, USA, NASA Goddard Earth Science Data and Information Services Center. doi: https://doi.org/10.5067/AJMZO5O3TGUR, accessed by March, 2020

Sun, Y., Frankenberg, C., Jung, M., Joiner, J., Guanter, L., Köhler, P., & Magney, T. (2018). Overview of Solar-Induced chlorophyll Fluorescence (SIF) from the Orbiting Carbon Observatory-2: Retrieval, cross-mission comparison, and global monitoring for GPP. *Remote Sensing of Environment, 209,* 808-823

Zhao, M., Heinsch, F.A., Nemani, R.R., & Running, S.W. (2005). Improvements of the MODIS terrestrial gross and net primary production global data set. *Remote Sensing of Environment*, *95*, 164-176